

DIAGNOSTIC DIAGRAMS AND TRANSFER FUNCTIONS FOR OCEANIC WAVE-GUIDES

BY FLAVIAN ABRAMOVICI*

ABSTRACT

The variation of frequency F as a function of wave number K and the associated spectral transfer function are computed for different modes in a complex oceanic wave-guide. The model consists of a fluid layer resting upon a three-layer elastic half-space. The layers and the half-space are homogeneous.

The comparison of theoretical results with measured power spectra for two records taken in the Pacific Ocean shows qualitative agreement stressing strongly the role of the leaking compressional organ-pipe modes which are not continuations of normal modes beyond cutoff frequency.

The mathematical procedure consists in the integration of the second-minor propagator equation of Gilbert and Backus (1966). The determinant representing the secular function is computed directly rather than by summing the products of its elements. This improves both accuracy and computing time. The integration can be reduced to that of a third-order nonlinear differential system which, for $K = 0$, splits into two Riccati equations.

The (F, K) -diagram corresponding to every mode is obtained by a technique based on properties of similar diagrams for simple oceanic and continental structures.

INTRODUCTION

The mode theory (see Pekeris, 1948) has been extensively used in studying elastic wave propagation in models consisting of one layer over a homogeneous half-space.

When the disturbance originates from a discrete source, the quantities defining the motion, like displacements, particle-velocity, etc. are represented as superpositions of free oscillations of the system. The corresponding frequencies are solutions of an eigen-value problem and are obtained as roots of a secular equation.

The roots which are real and correspond to phase-velocities lower than the shear-velocity in the half-space, give the normal or locked modes. The entire energy is trapped in the wave-guide and therefore these modes are predominant at large distances from the source.

The other roots of the secular equation, which are in general complex, give rise to the leaking modes. In this type of motion, energy is transmitted to the half-space so that the amplitude decreases both with time and distance. The attenuation depends upon the imaginary part of the complex frequency.

Leaking mode propagation in a layered liquid was investigated by Rosenbaum (1960) and extended to a simple oceanic wave-guide by Phinney (1961). A systematic study of the frequency as function of wave number (diagnostic diagrams) and

*On leave from the Department of Applied Mathematics, The Weizmann Institute of Sciences, Rehovoth, Israel.

detailed numerical results for simple continental and oceanic structures were given by Gilbert (1964).

Some of the leaking modes are continuations of normal modes below the cutoff frequency.

They start either as solutions of the Rayleigh equation, the frequency vanishing when the wave number goes to zero, or as organ-pipe modes of compressional or shear type. Having higher group velocities, they are present in the earlier portions of the seismograms. These leaking modes are associated with the oscillatory motion following the arrival of P or S at moderate epicentral distances (Oliver and Major, 1960; Oliver, 1961; Su and Dorman, 1965). They are also recorded in model experiments (Gilbert and Laster, 1962).

There are other roots of the secular equation, which are not continuations of locked modes. They start also as organ-pipe modes. The corresponding group velocity is very low so that these modes are present only in the later portions of the seismograms and therefore their attenuation is very strong. The contribution of these modes is important however in microseisms, in the neighbourhood of the generating area.

The object of this paper is to investigate the modes of all types in a complex oceanic wave-guide. The dispersion relationship will be presented mainly as diagnostic diagrams, i.e., graphs of the real and imaginary parts of the complex frequency as functions of real wave number.

We also investigate the relative contribution of different modes to the response of an oceanic structure excited by a random pressure field. Following Hasselmann's theory (Hasselmann, 1963) we represent the response of the wave-guide to a continuous random forcing field in terms of functions expressing average properties of the quantities describing the motion. Such a function is the power spectrum. When the power spectrum of the exciting field is known, that of the response can be calculated in a first approximation. Otherwise we can calculate only the transfer function which is entirely determined by the properties of the wave guide. If the power-spectrum of the external pressure field has a smooth variation, the transfer-function will represent, at least qualitatively, the power spectrum of the response.

In order to compare theoretical and observational results, we consider two power-spectra corresponding to records taken at the bottom of the Pacific Ocean. The complex structures used in the theoretical calculations correspond to stations near the locations of the recording instruments. The results of this comparison are given in Section 4.

The first step of this calculation consists in finding the variation of frequency with wave number. The results for several leaking and locked modes are presented in Section 3 in the form of diagnostic diagrams. Group and phase velocities are also presented as functions of the frequency. Some of the mathematical steps are given in Section 1 whereas others as well as some of the formulae are given in the Appendices. The computational procedure is outlined in Section 2.

(1) *Mathematical solution.* We consider an oceanic wave-guide consisting of a homogeneous fluid layer of depth H_2 resting upon a heterogeneous solid layer of depth H_1 . The whole structure, which is of depth $H = H_1 + H_2$, is welded to a homogeneous solid half-space. We take a cartesian system of coordinates having

the origin at the interface between the wave-guide and the half-space. The x -axis is situated in the plane of this interface and so is the z -axis. The y -axis is perpendicular to this plane and points upwards (Figure 1).

The quantities related to the half-space will be denoted using the index 0, those belonging to the fluid layer, using the index 2.

We want to compute the power spectrum of the vertical displacement at the bottom of the fluid layer in the assumption that a random pressure field is acting on the surface of the wave-guide (Hasselmann, 1963). Supposing that the pressure field is homogeneous and stationary, it can be represented by the Fourier-Stieltjes integrals

$$p(x, t) = \iint e^{i(kx-\omega t)} dP(k, \omega). \tag{1}$$

The pressure field is supposed to be independent of z like all the other quantities involved in this problem.

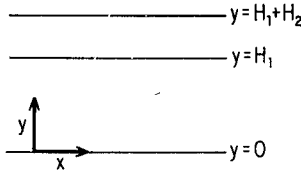


FIG. 1. Assumed model for a complex oceanic wave guide.

Representing the components of displacement s_y, s_x and of stress $\tau_{yy}, \tau_{yx}, \tau_{xx}$ also as Fourier-Stieltjes integrals

$$\int e^{i(kx-\omega t)} ds_y, \dots \tag{2}$$

we find from the momentum equations and Hooke's law that formally $ds_y, ds_x, d\tau_{yy}, d\tau_{yx}$ in the solid layer are solutions of the fourth-order differential system (Gilbert and Backus, 1966)

$$\frac{\partial}{\partial y} \begin{pmatrix} ds_y \\ ds_x \\ d\tau_{yy} \\ d\tau_{yx} \end{pmatrix} = \begin{pmatrix} 0 & \frac{K\lambda}{\lambda + 2\mu} & \frac{1}{\lambda + 2\mu} & 0 \\ -K & 0 & 0 & \frac{1}{\mu} \\ -\rho F^2 & 0 & 0 & K \\ 0 & -\rho F^2 + K^2 \left(\lambda + 2\mu - \frac{\lambda^2}{\lambda + 2\mu} \right) - \frac{K\lambda}{\lambda + 2\mu} & 0 & 0 \end{pmatrix} \begin{pmatrix} ds_y \\ ds_x \\ d\tau_{yy} \\ d\tau_{yx} \end{pmatrix}. \tag{3}$$

The quantities appearing here are non-dimensional. They are obtained by the following substitutions:

$$\begin{aligned}
 s &\rightarrow s/H, & y &\rightarrow y/H, & K &\rightarrow kH, & F &\rightarrow \omega H/\beta_0 \\
 \rho &\rightarrow \rho/\bar{\rho}, & \lambda &\rightarrow \lambda/(\bar{\rho}\beta_0^2), & \mu &\rightarrow \mu/(\bar{\rho}\beta_0^2), & \tau &\rightarrow \tau/(\bar{\rho}\beta_0^2).
 \end{aligned}
 \tag{4}$$

$\bar{\rho}$ is the mean density, β_0 the shear velocity in the half-space.

In the fluid layer, the solution is

$$\begin{aligned}
 ds_y &= \frac{\nu_2}{2} [e^{\nu_2(y-1)} dB + e^{-\nu_2(y-1)} dC] \\
 d\tau_{yy} &= -\frac{\rho_2 F^2}{2} [e^{\nu_2(y-1)} dB - e^{-\nu_2(y-1)} dC] \\
 \nu_2 &= (K^2 - F^2/\alpha_2^2)^{1/2}.
 \end{aligned}
 \tag{5}$$

F is the non-dimensional frequency and α_2 the non-dimensional sound velocity in the fluid layer.

The solution in the solid layer is a linear combination of two independent solutions (s' , τ') and (s'' , τ''):

$$\begin{aligned}
 ds &= s' dA' + s'' dA'' \\
 d\tau &= \tau' dA' + \tau'' dA''.
 \end{aligned}
 \tag{6}$$

The coefficients dA' , dA'' , dB , dC are determined from the boundary conditions: (1) at the surface ($y = 1$)

$$d\tau_{yy} = -\frac{\rho_2 F^2}{2} [dB - dC] = -dP\dagger
 \tag{7}$$

(2) at the fluid-solid interface ($y = y_1 = H_1/H$)

$$\begin{aligned}
 s_y' dA' + s_y'' dA'' &= \frac{\nu_2}{2} [e^{\nu_2(y_1-1)} dB + e^{-\nu_2(y_1-1)} dC] \\
 \tau_{yy}' dA' + \tau_{yy}'' dA'' &= -\frac{\rho_2 F^2}{2} [e^{\nu_2(y_1-1)} dB - e^{-\nu_2(y_1-1)} dC] \\
 \tau_{yx}' dA' + \tau_{yx}'' dA'' &= 0.
 \end{aligned}
 \tag{8}$$

The solution of (7)-(8) is:

$$dA' = G_A'/G, \quad dA'' = G_A''/G, \quad dB = G_B/G, \quad dC = G_C/G
 \tag{9}$$

† Here dP is the actual pressure divided by $\bar{\rho}\beta_0^2$.

where

$$G = uG_{(12)}^{(34)} + vG_{(12)}^{(14)}$$

$$u = \nu_2 \cosh [(y_1 - 1)\nu_2], \quad v = \rho_2 F^2 \sinh [(y_1 - 1)\nu_2]. \tag{10}$$

$G_{(12)}^{(34)}$ and $G_{(12)}^{(14)}$ are the minors formed with the third and fourth rows and first and fourth rows respectively out of the matrix

$$\begin{pmatrix} s_y' & s_y'' \\ s_x' & s_x'' \\ \tau_{yy}' & \tau_{yy}'' \\ \tau_{yx}' & \tau_{yx}'' \end{pmatrix}. \tag{11}$$

G_A', G_A'', G_B, G_C are the determinants obtained from G by replacing one of the columns by

$$\begin{pmatrix} \frac{2}{\rho_2 F^2} dP \\ 0 \\ 0 \\ 0 \end{pmatrix}. \tag{12}$$

The result is

$$G_{A'} = \nu_2 \tau_{yx}'' dP, \quad G_{A''} = -\nu_2 \tau_{yx}' dP$$

$$G_B = -\frac{e^{-\nu_2(y_1-1)}}{\rho_2 F^2} [\nu_2 G_{(12)}^{(34)} - \rho_2 F^2 G_{(12)}^{(14)}] dP$$

$$G_C = \frac{e^{\nu_2(y_1-1)}}{\rho_2 F^2} [\nu_2 G_{(12)}^{(34)} + \rho_2 F^2 G_{(12)}^{(14)}] dP. \tag{13}$$

The final form for the vertical displacement at the bottom of the fluid layer is:

$$s_y = \iint e^{i(kx-\omega t)} \frac{\nu_2 G_{(12)}^{(14)}}{G} dP. \tag{14}$$

As has been shown by Hasselmann, the response of the system to a homogeneous and stationary random pressure field is not stationary. The time derivative of the power spectrum of the displacement $E_{s_y}(K)$ is given by

$$\frac{\partial E_{sy}^{(n)}(K)}{\partial t} = T_{sy}^{(n)}(K) E_p(K, F_n) \quad (15)$$

where $T_s^{(n)}(K)$ is the so-called transfer function

$$T_{sy}^{(n)}(K) = 2\pi \left| \frac{\nu_2 G\left(\frac{1}{2}\right)}{F_n \left(\frac{\partial G}{\partial F}\right)_{F=F_n}} \right|^2. \quad (16)$$

The index n indicates the n th mode, F_n being the eigen-frequency for this mode, corresponding to the given value of K . When the pressure field is not homogeneous, formula (15) is no longer valid. For the simple case in which the power spectrum of the pressure field $E_p(K, F_n)$ is constant inside a generating area and zero outside, Hasselmann gives an expression for the power spectrum with respect to frequency which in our case is:

$$E_{sy}^{(n)}(F) = \frac{A}{R} \tilde{T}_{sy}^{(n)}(F) E_p(K_n, F) \quad (17)$$

where now the transfer function is

$$\tilde{T}_{sy}^{(n)}(F) = \frac{K}{v_n^2} T_{sy}^{(n)}(K_n) \quad (18)$$

$T_{sy}^{(n)}(K_n)$ being given by (16). v_n is the group velocity.

In order to calculate the transfer function we have to find the eigen-frequencies for every mode, i.e., we have to solve the secular equation

$$G = G(K, F) = 0 \quad (19)$$

G being given by (10). The roots may be real or complex and may be situated on different sheets of the Riemann surface associated with the secular function G . This is shown in detail by Gilbert (Gilbert, 1964). There are four Riemann sheets corresponding to the four different combinations of signs of the real parts of the square roots

$$(K^2 - F^2/\alpha_0^2)^{1/2}, \quad (K^2 - F^2)^{1/2}. \quad (20)$$

The complex F -plane is supposed to be cut along the real axis from F and F/α_0 to infinity and from $-F$ and $-F/\alpha_0$ to minus infinity. The real roots on the $(+, +)$ -sheet, of modulus less than K give the locked modes, which correspond to the classical surface waves. The roots situated on the other sheets give the leaking modes.

(2) *Numerical calculations.* In the process of finding the eigen-frequencies, the most time-consuming is the calculation of $G\left(\frac{34}{12}\right)$ and $G\left(\frac{14}{12}\right)$ appearing in (10). The direct method would be to integrate the differential system (3) twice, in order to get the two required independent solutions. The starting values for these integra-

tions are given in Appendix B. Having the values of these solutions for $y = y_1$, one can compute the desired second-order determinants. By doing so, accuracy may be lost due to cancellation. An alternative procedure (Gilbert and Backus, 1966) is to compute the second order determinants directly from the sixth order differential system they satisfy.† This not only will improve the accuracy of the numerical results but will also save computing time. The computing time can further be reduced as the sixth-order differential system can be replaced by a third-order one. The proof of this is given in Appendix A. The third-order system is non-linear but this does not cause any problems as far as the Runge-Kutta method is concerned. The only trouble might come from the singularities introduced by taking ratios of the solutions of the sixth order system. In the neighborhood of such singularities the inverse of the solutions can be computed using the corresponding differential system obtained from the initial one in an obvious way.

As it is shown in Appendix A, for $K = 0$ the third-order system splits into two first-order Riccati equations, one for the P waves, the other for the S waves.

The practical procedure to find the leaking modes is to compute first the initial roots corresponding to $K = 0$ and to follow them as K varies (Gilbert, 1964). Accordingly, our computational procedure involves two steps.

(a) *Initial roots.* There are two kinds of initial roots. One of them is related to the solutions of the Rayleigh equation, situated on different Riemann sheets. When K tends to zero, the frequency F tends also to zero but the ratio F/K is finite and not zero. The real root on the $(+, +)$ -sheet gives the familiar Rayleigh mode \tilde{S}_{++} . The same root appears on the $(-, -)$ -sheet, giving rise to the \tilde{S}_{--} -mode. On the remaining sheets there are either two pairs of complex conjugate or four real roots. For the structures used in our numerical calculation the last case takes place. By finding these roots we get the starting points for the mode \tilde{P}_{+-} and \tilde{P}_{-+} .

The other type of initial roots are related to the so-called "organ-pipe" modes for which the frequency is not zero for $K = 0$. These roots are obtained as solutions of the equations

$$G_1 \equiv U_3/U_1 = 0 \quad (21)$$

$$G_2 \equiv u(U_4/U_1) - v = 0 \quad (22)$$

where u, v are given by (10) and $U_3/U_1, U_4/U_1$ are solutions of (A.23) and (A.24) (Appendix A). The roots of (21) give the shear organ-pipe modes and are on the $(+, -)$ and $(-, -)$ Riemann sheets. These modes are denoted Σ_i^{+-} and Σ_i^{--} respectively. The roots of (22) correspond to the compressional organ-pipe modes and appear on the $(-, +)$ and $(-, -)$ sheets. These modes are denoted Π_i^{-+} and Π_i^{--} . Since in both cases we have to find the complex zeros of a complex function G_1 or G_2 , a computer-program was set up finding first the curves in a finite region of the complex plane of the independent variable, such that the real and imaginary parts respectively of the considered function are zero. The intersection of these curves is taken as a first approximation and using Newton's method, the

† The sixth-order system and the starting values for the solution are given in Appendix B.

desired roots are found. All the derivatives involved in this calculation are computed to the same accuracy as the functions themselves. They are solutions of the differential system obtained from the initial one by taking derivatives with respect to the frequency F .

(b) *Roots for $K \neq 0$.* Once the initial root is known for a particular mode, the variation of the frequency F with K is obtained by increasing K and computing F by iterations. The first approximation is obtained by extrapolation

$$F(K_1) = F(K_0) + (K_1 - K_0) \left(\frac{dF}{dK} \right)_0 \quad (23)$$

K_0 being the previous value of K and K_1 the new one. The derivative dF/dK , the absolute value of which is the group velocity, is obtained from

$$\frac{dF}{dK} = \frac{dG/dK}{dG/dF} \quad (24)$$

The derivatives of G are obtained integrating the corresponding differential system (see Appendix B).

In order to make the calculation of F as automatically as possible, several rules concerning the behaviour of the roots must be taken into account. One of them is that all the complex roots of the secular equation are simple. They are complex conjugate so that when the real axis in the F -plane is reached they give rise to double roots. The real axis can be reached in one of the following two circumstances. Either it is crossed for $K > K/\alpha_0$ which means that both cuts are intersected and the root passes from the $(+, -)$ -sheet to $(-, +)$ sheet or vice-versa and is further complex. Or, the real axis is reached at a point $F < K$. In this case, by increasing K we get two simple real roots, one moving leftwards relative to K and the other rightwards. The right root will finally overtake K and will change sheets. If it was on the $(+, -)$ -sheet, it will enter the top sheet at the cutoff value, becoming one of the locked modes. If it was on the $(-, -)$ -sheet, it will go over to the $(-, +)$ -sheet. The left root will stay all the time on the same sheet, the distance to K increasing.

(3) *Diagnostic diagrams.* We consider two oceanic structures corresponding to stations Hilo 19 (Pollard and Eaton, 1963) and Hilo 31 (Shor and Pollard, 1964) in the Pacific Ocean near Hawaii. The two models have the same distribution of densities and ratios of wave velocities.† The corresponding parameters are given in Table 1.

The relationship between the frequency F and the wave-number K can be represented either in the form of diagnostic diagrams or by plotting the group velocity and the phase velocity for every mode. The group velocity g is defined as the absolute value of the derivative of the real part of the frequency F_r , with respect to the wave number K :

$$g = \left| \frac{dF_r}{dK} \right| \quad (25)$$

† We are indebted for these data to Dr. Don Helmberger of the Scripps Institution of Oceanography (private communication).

and the phase velocity U is:

$$U = \begin{cases} F_r/K & \text{if } dF_r/dK > 0 \\ -F_r/K & \text{if } dF_r/dK < 0. \end{cases} \quad (26)$$

When the phase velocity is positive, individual crests advance as energy travels away from the source, otherwise they regress. As the group velocity is always positive it can be identified with the velocity of energy transport with one restriction: it must be less than the highest wave-velocity of the structure. This is always true

TABLE 1
VARIATION OF DENSITY AND WAVE VELOCITIES FOR HILO 19 AND
HILO 31

Model	H	ρ	α	β
Hilo 19	4.65	1	1.50	—
	0.27	1.4	3.00	1.12
	3.18	2.4	4.18	2.03
	5.17	2.8	6.89	3.91
	∞	3.2	8.13	4.78
Hilo 31	4.39	1	1.50	—
	1.0	1.4	4.20	1.57
	1.4	2.4	6.06	2.94
	4.3	2.8	6.83	3.88
	∞	3.2	8.71	5.12

for those portions of the diagnostic diagrams which are permissible (Gilbert, 1964) namely:

- I. (+, +)-sheet $F_r < K$
- II. (+, -)-sheet $K < F_r < \alpha_0 K$
- III. (-, -)-sheet $\alpha_0 K < F_r$. (27)

In Figures 12–19 group and phase velocities are represented only for these values of the frequency. The connection of leaking to locked modes is seen clearly on Figures 12–14 and 16–18.

Diagnostic diagrams are represented in Figures 2–11. For each mode there are two curves, one for the real part F_r , the other for the imaginary part F_i . When F is complex, only the root in the first quadrant is shown. The passage from one Riemann sheet to another is marked either by a vertical line indicating the crossing of both cuts in the frequency plane or by an arrow, when the (+ +)-sheet or (- +)-sheet are entered.

The diagrams for the \bar{P}_{+-} -mode are represented in Figure 2. The curves are very similar for the two models considered and their general behaviour is somehow between those corresponding to a simple oceanic structure and those for a simple

continental one (Gilbert, 1964). The starting velocity of F_r with respect to K equals the smaller real root of the Rayleigh equation on the $(+ -)$ -sheet, like in the case of a simple continental structure. F_r and F_i have almost the same values respectively, for small K . When K increases, F_r for Hilo 19 is higher and consequently so is the phase velocity. On the contrary, F_i is higher for Hilo 31, which means that in this case the attenuation is slightly higher. As K increases, the root in the first quadrant and its conjugate in the fourth one approach the real axis giving rise to a double root. For further values of K , F_r has two branches, the lower one staying on the $(+ -)$ -sheet whereas the higher one takes over the shear branch-

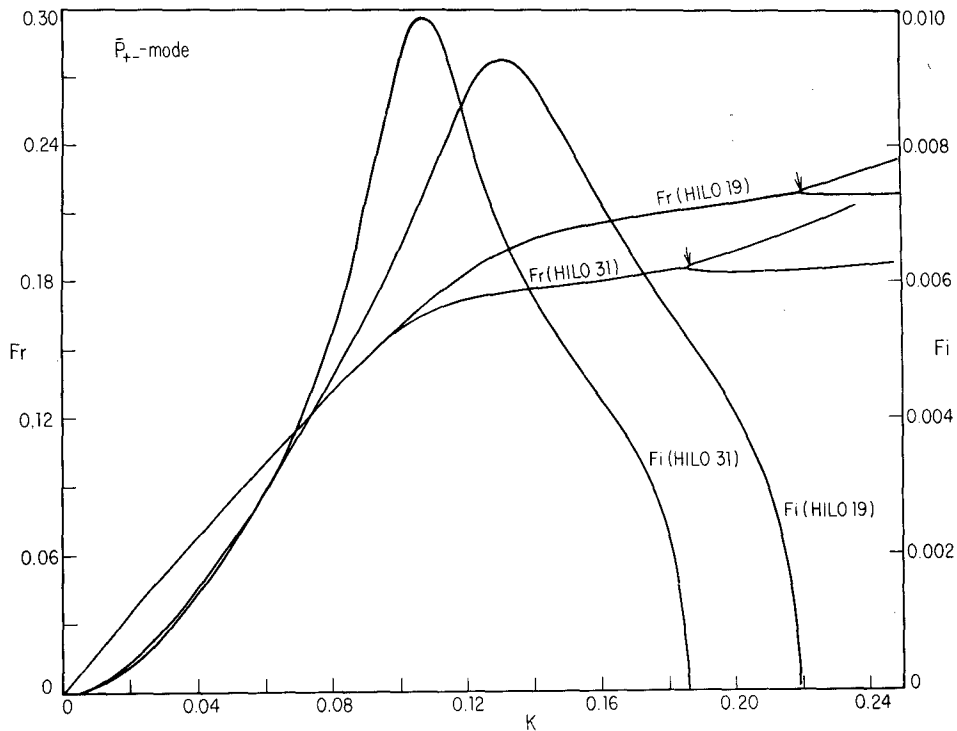


FIG. 2. Diagnostic diagrams for the \bar{P}_{+-} -mode.

point K and enters the $(+, +)$ -sheet becoming the second locked mode or the first shear mode. The values of F_r at both the double point and the cutoff are higher for Hilo 19 and correspond to higher wave-numbers. The group velocity has, in the earlier portions of the diagrams, numerical values which are larger than α_0 , the compressional waves velocity in the half-space, which is the highest wave velocity in the considered structures. If, however, we consider only the permissible values on the $(+ -)$ -sheet, interpretation of the group velocity as the energy-transport velocity is meaningful. Indeed, starting from $K \simeq .04$, F_r for both models is less than $K\alpha_0$ and the group velocity is less than 1.701, the non-dimensional value of α_0 as we can see also in Figure 12.

The diagrams for the \bar{P}_{-+} mode are given in Figure 3. This mode starts on the nonpermissible $(-, +)$ -sheet. The group-velocity corresponds to the larger real root of the Rayleigh equation on this sheet. As K increases, F_r is almost the same for the two models, except in the neighbourhood of the point at which the $(+, -)$ -sheet is entered for Hilo 31. F_i however is not the same. It is much higher for Hilo 19 on the $(-, +)$ -sheet. On the contrary, on the $(+ -)$ -sheet it is much higher for Hilo 31, which means that this mode presents a strong attenuation for Hilo 31 and a relatively small one for Hilo 19. The wave number and frequency at which the $(+ -)$ -

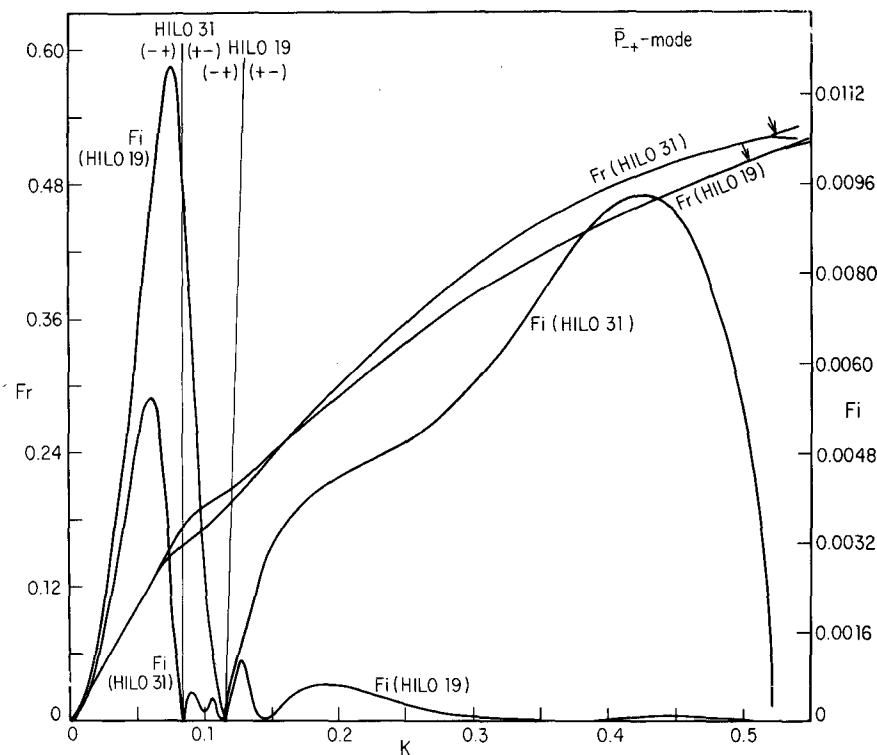


FIG. 3. Diagnostic diagrams for the \bar{P}_{-+} -mode.

sheet is entered are smaller for Hilo 31. It has to be noted that the $(+ -)$ -sheet is entered only once, F staying on this sheet as K increases, contrary to the behaviour of the \bar{P}_{-+} mode for the simple oceanic wave-guide (Gilbert, 1964). There the $(- +)$ and $(+, -)$ sheets are changed several times, whereas in the cases of complex oceanic wave guides presented here, this is not so. The real part of the frequency F_r is smaller for Hilo 31 on the $(- +)$ -sheet but on the $(+ -)$ -sheet the situation is reversed. The wave number and frequency at the double point and cutoff are less for Hilo 19, contrary to \bar{P}_{-+} . The group velocity for both models is lower than the compressional waves velocity, when the $(+ -)$ -sheet is entered.

The diagrams for the mode Π_1^{-+} are given in Figure 4. Like \bar{P}_{-+} , they start on the $(- +)$ -sheet and after a while cross both branch-cuts and enter the $(+ -)$ -sheet.

Now, for Hilo 19 is F_i smaller on the $(-+)$ -sheet and larger on the $(+-)$ -sheet and the crossing of the branch-cut is made for Hilo 19 at lower frequencies and wave numbers. On the $(+-)$ -sheet F_i for both models is small, F_r for Hilo 31 being much larger. F_i for both models has a point of sharp change of curvature near the crossing of the branch cuts. This is not a discontinuity in the derivative as it would seem to be. A small portion of the F_r -curve for Hilo 19 is represented on an enlarged scale and it shows clearly that although it is a strong change in curvature, it is a continuous one. The derivative of F_r with respect to K starts having very small positive values, then it increases sharply near $K = 0.10$, it keeps more or less a

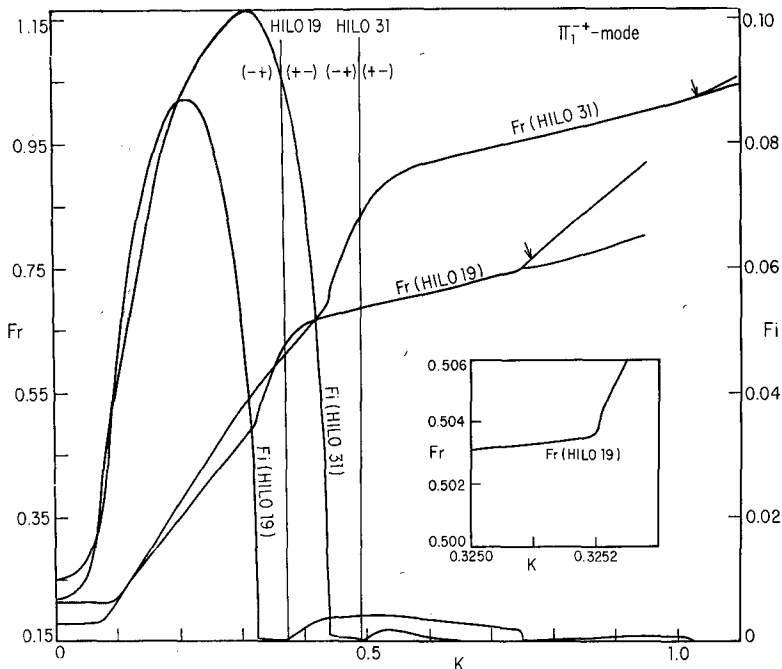


FIG. 4. Diagnostic diagrams for the Π_1^{+-} -mode. In the right corner is shown an enlarged portion of F_r for Hilo 19.

constant value, has again a sharp increase near $K = 0.32$ for Hilo 19 and $K = 4.4$ for Hilo 31 and then decreases steadily as the branch-cuts are crossed. After entering the $(+-)$ -sheet its numerical value is less than the highest wave velocity in the structure and its interpretation as the group velocity for this portion of the diagram is meaningful. After entering the $(+,+)$ -sheet this mode becomes the fourth shear locked mode for Hilo 19 but the fifth for Hilo 31.

Figure 5 shows the second compressional organ-pipe mode Π_2^{+-} starting on the non-permitted sheet $(-+)$. Contrary to Π_1^{+-} , here F_i for Hilo 19 is much higher. On the $(+,+)$ -sheet it will give the fifth shear locked mode, whereas that for Hilo 31 will give the fourth one. The behaviour of F_i is different especially for lower values of K . Similar to \tilde{P}_{-+} , there is only one change of Riemann sheets and not two as for a simple oceanic wave-guide (Gilbert, 1964).

The first two shear organ-pipe modes Σ_1^{+-} and Σ_2^{+-} starting on the $(+, -)$ -sheet are given in Figures 6-7. Their behaviour is similar to that for a simple continental structure, there are no changes of Riemann sheets, therefore no double points except that at which the frequency becomes real. For both Σ_1^{+-} and Σ_2^{+-} , F_r is larger for Hilo 31 and goes to the third shear locked mode on the top Riemann sheet. F_i however has a different behaviour, it is larger for Hilo 19 for most values of K and only in the final part of the diagram it becomes smaller and vanishes for a lower wave number. The group velocity for both modes starts by being very low and

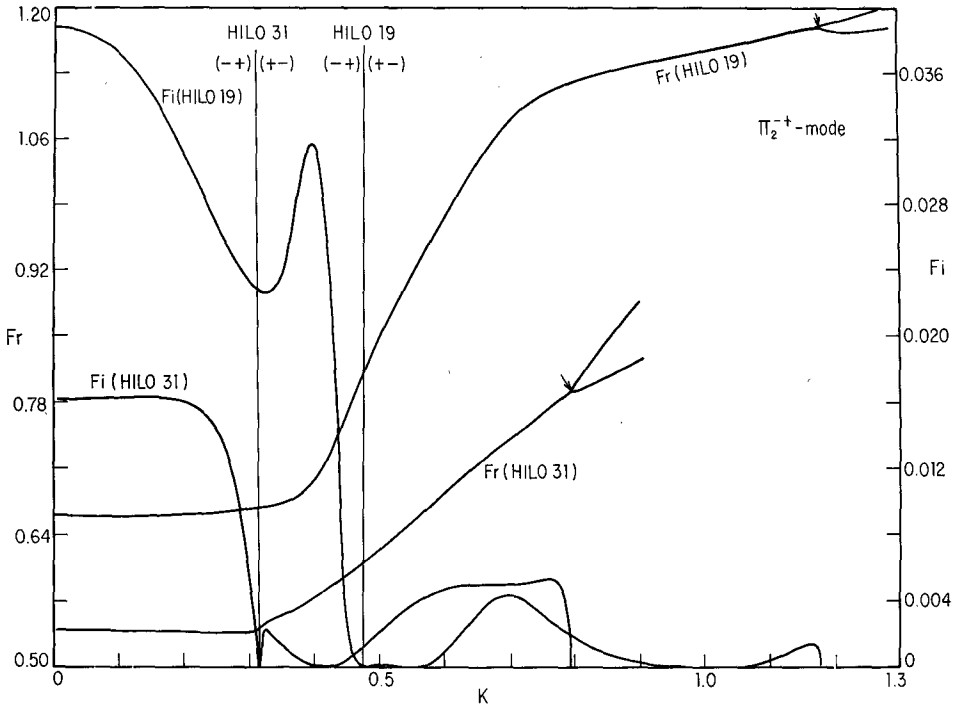


FIG. 5. Diagnostic diagrams for the Π_2^{+-} -mode.

increases gradually. It is always less than the largest shear velocity present in the structure for all the permitted values of the frequency.

The first two compressional organ-pipe modes on the $(-, -)$ -sheet are shown in Figures 8-9. As it can be seen in Figure 8, except for a small region, F_i is higher for Hilo 19 and vanishes for a higher wave number. There are no double roots except when the frequency becomes real. Beyond the double root there are two branches, one staying on the $(-, -)$ -sheet, the other entering the $(-, +)$ -sheet when the branch-point K is reached. On this branch F_r for Hilo 31 becomes higher but as K increases and F_r for Hilo 19 enters the $(-, +)$ -sheet, the curves almost coincide. The general behaviour of the diagrams is the same for the two models. We remark the negative phase velocity in Figures 15 and 19. For Π_2^{--} in Figure 9 again the behaviour is more or less similar. Both F_r and F_i are much higher for Hilo 19.

Figures 10-11 show the first two shear organ-pipe modes Σ_1^{--} and Σ_2^{--} on the $(-, -)$ -sheet. The real part of the frequency is higher now for Hilo 31 for both Σ_1^{--} and Σ_2^{--} . F_i is higher for Hilo 31 in the first mode and lower in the second. The double roots on the real axis correspond to lower frequency for Hilo 19. One portion of the F_r -curve for Σ_1^{--} is shown on enlarged scales for K and F_r , respectively.

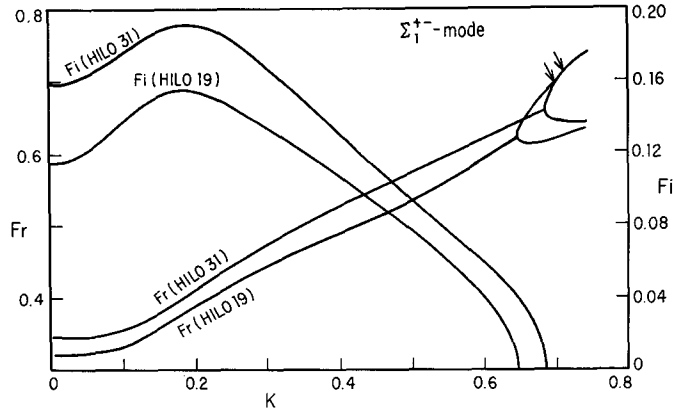


FIG. 6. Diagnostic diagrams for the Σ_1^{+-} -mode.

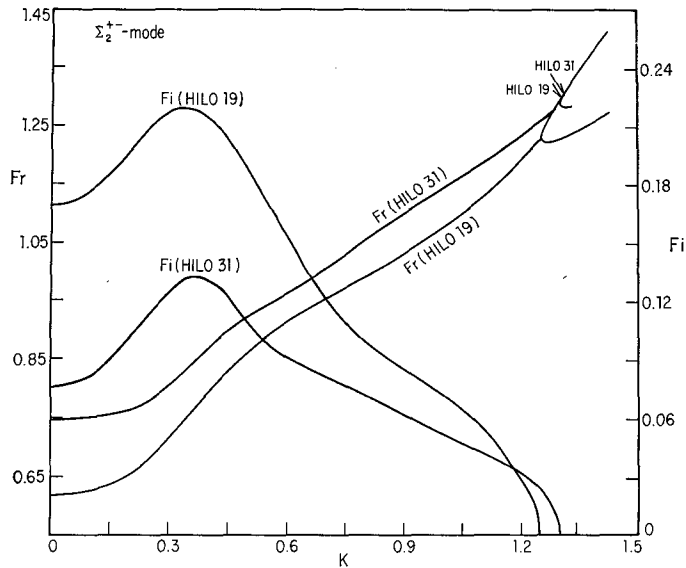


FIG. 7. Diagnostic diagrams for the Σ_2^{+-} -mode.

(4) *Power spectra.* For every mode for which the variation of frequency with wave-number is established, the power spectrum $E_{s_y}^{(n)}(F)$ can be computed using (17) if the power spectrum of the external pressure field $E_p(K_n, F)$ is known. Otherwise, in the assumption that $E_p(K_n, F)$ has a smooth variation, the behaviour of $E_{s_y}^{(n)}(F)$ is determined by that of the transfer function $\hat{T}_{s_y}^{(n)}(F)$, the presence of

$E_p(K_n, F)$ manifesting itself only by shifting a little the points of relative maximum or by changing slightly the values of $E_{s_y}^{(n)}(F)$.

The continuous lines in Figures 20, 22 represent power density spectra for two records taken by submerged instruments in the Pacific Ocean (Bradner and Dodds,

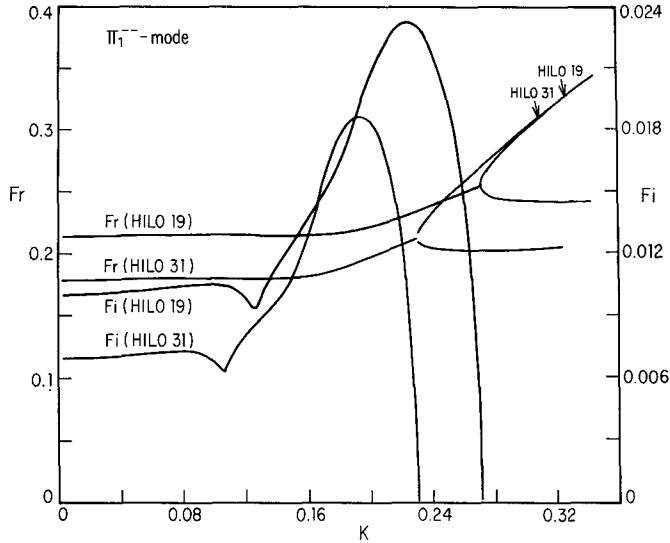


FIG. 8. Diagnostic diagrams for the II₁⁻⁻-mode.

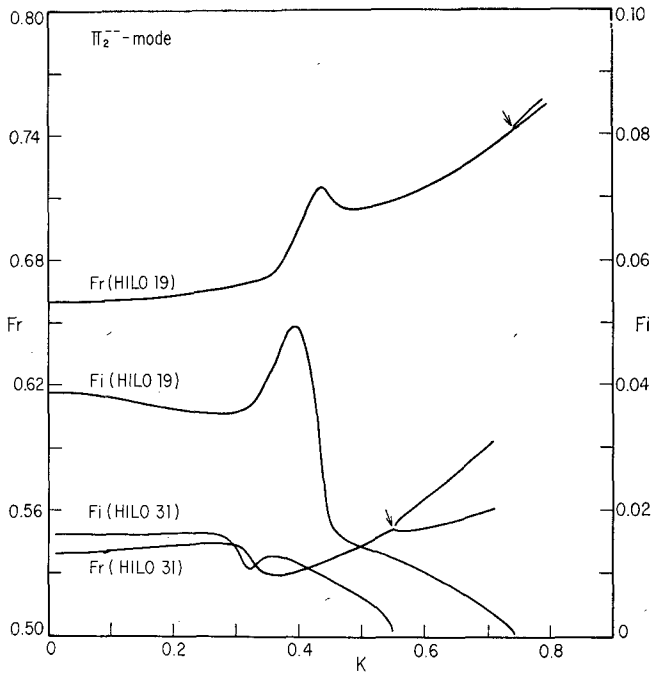


FIG. 9. Diagnostic diagrams for the II₂⁻⁻-mode.

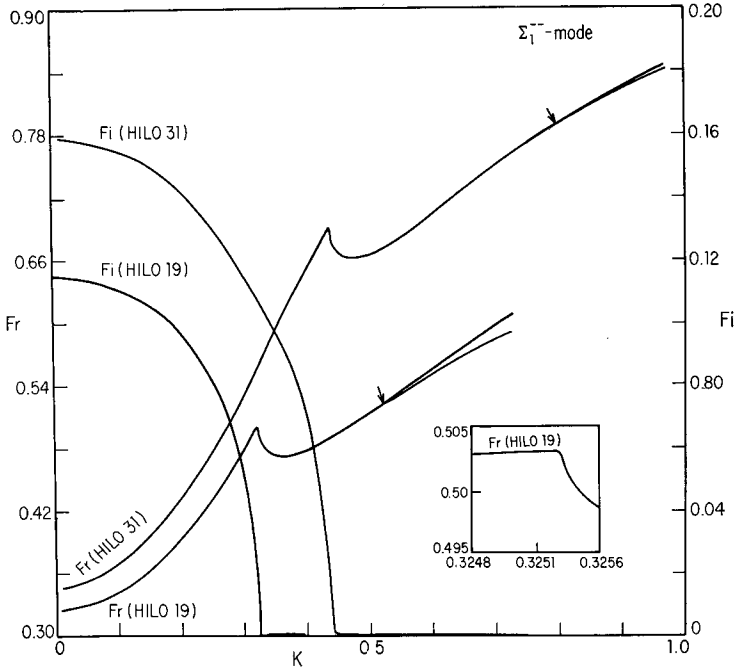


FIG. 10. Diagnostic diagrams for the Σ_1^- -mode. In the right corner is shown an enlarged portion of Fr for Hilo 19.

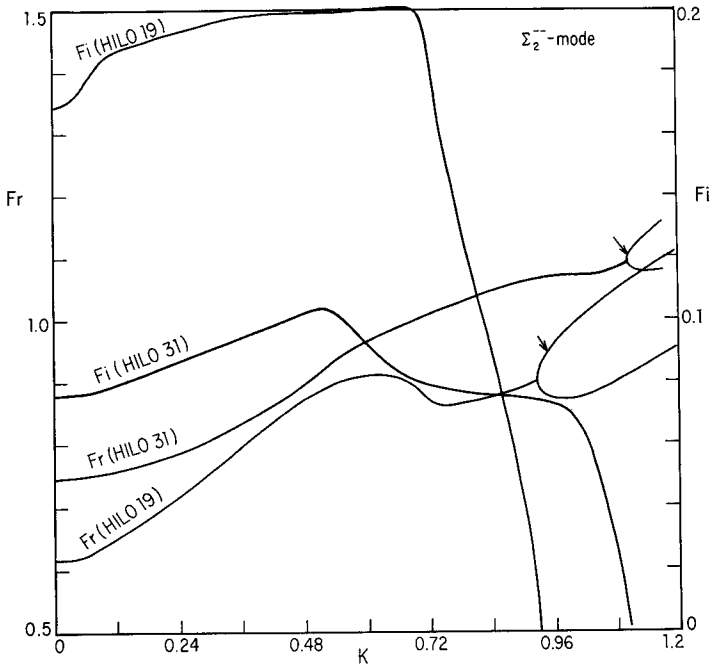


FIG. 11. Diagnostic diagrams for the Σ_2^- -mode.

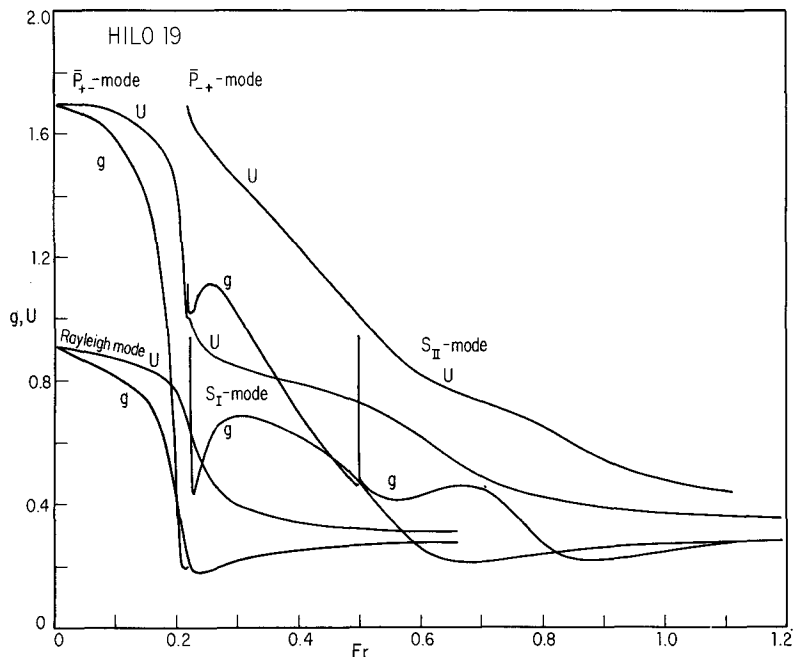


FIG. 12. Phase and group velocities U and g for the Rayleigh mode and for the first two shear modes and their continuations \bar{P}_{+-} and \bar{P}_{-+} respectively. The model is Hilo 19.

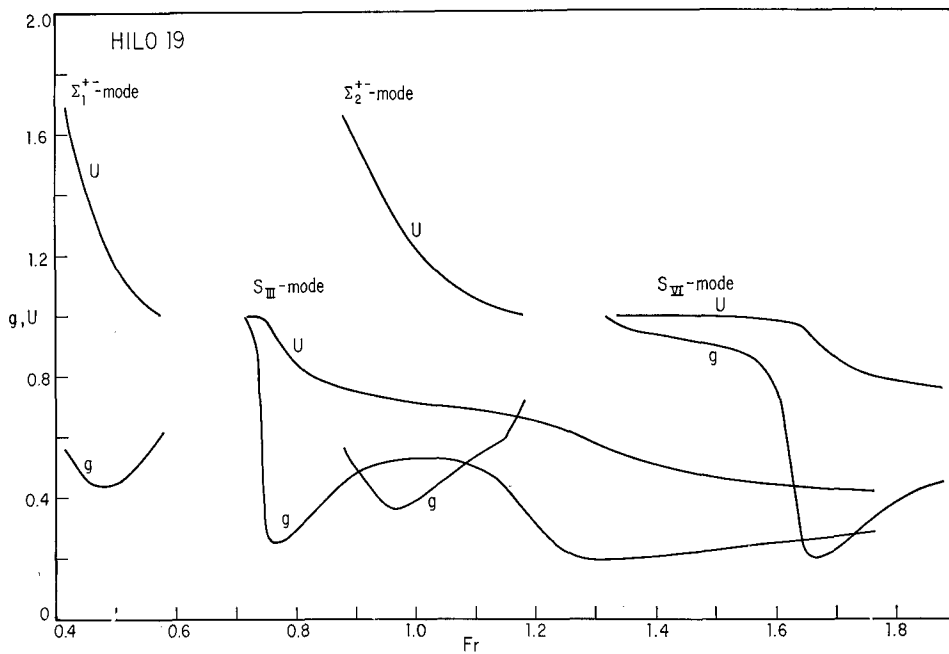


FIG. 13. Phase and group velocities U and g for the third and sixth shear modes and their continuations Σ_{1+-} and Σ_{2+-} respectively. The model is Hilo 19.

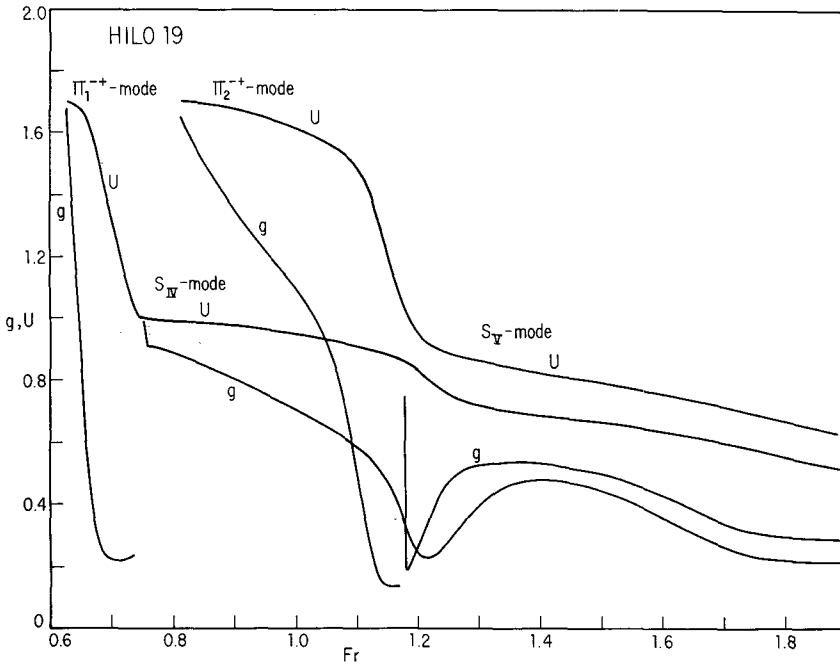


FIG. 14. Phase and group velocities U and g for the fourth and fifth shear modes and their continuations Π_1^{+-} and Π_2^{+-} respectively. The model is Hilo 19.

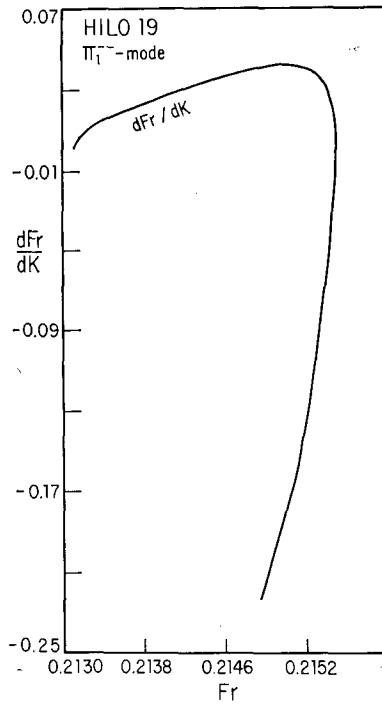


FIG. 15. The derivative dF_r/dK for the Π_1^{--} -mode. The model is Hilo 19. The group velocity is $g = |dF_r/dK|$.

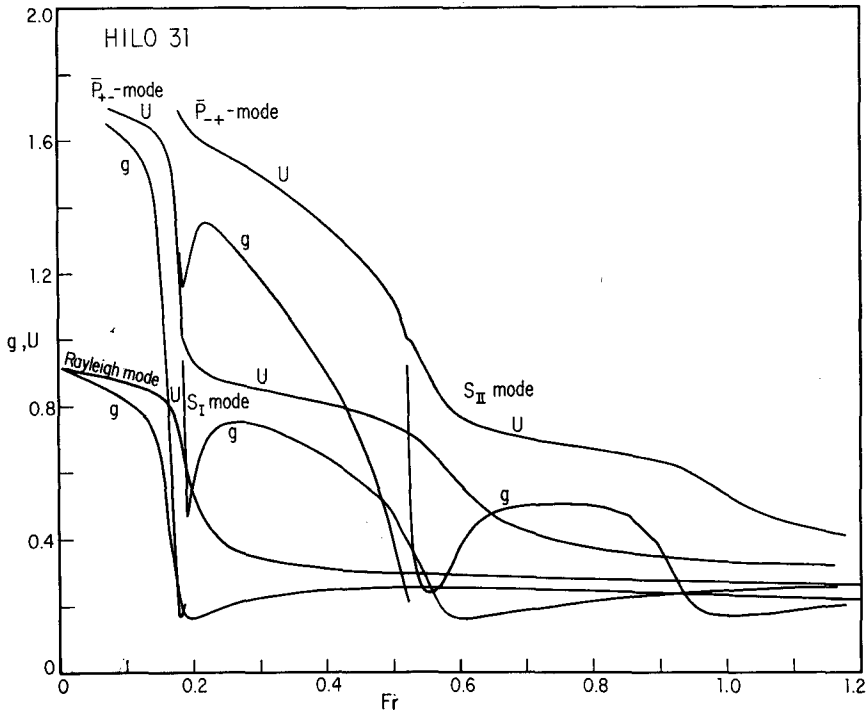


FIG. 16. Phase and group velocities U and g for the Rayleigh mode and for the first two shear modes and their continuations \bar{P}_{+-} and \bar{P}_{-+} respectively. The model is Hilo 31.

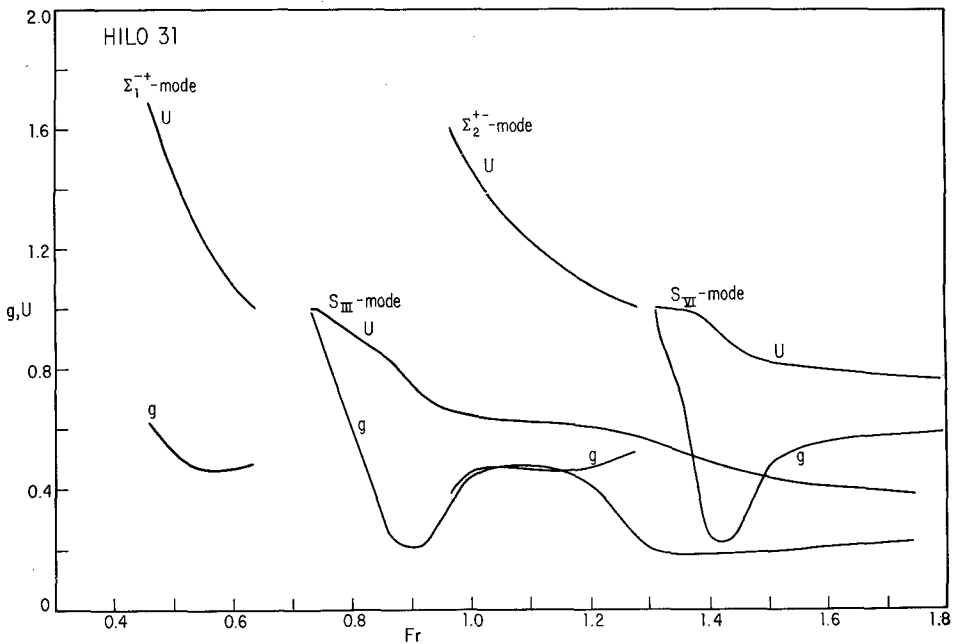


FIG. 17. Phase and group velocities U and g for the third and the sixth shear modes and their continuations $\Sigma_{1^{+-}}$ and $\Sigma_{2^{+-}}$ respectively. The model is Hilo 31.

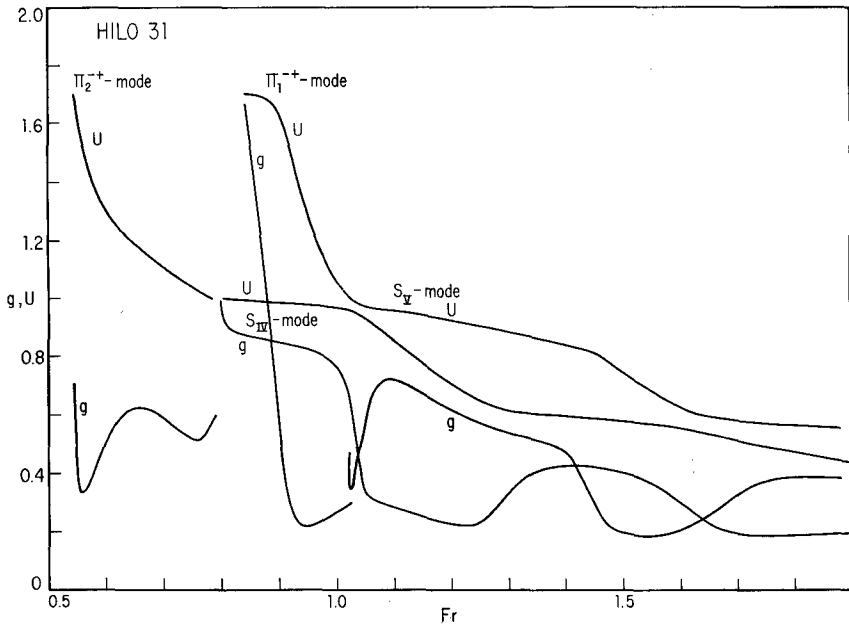


FIG. 18. Phase and group velocities U and g for the fourth and fifth shear modes and their continuations Π_2^{+-} and Π_1^{+-} respectively. The model is Hilo 31.

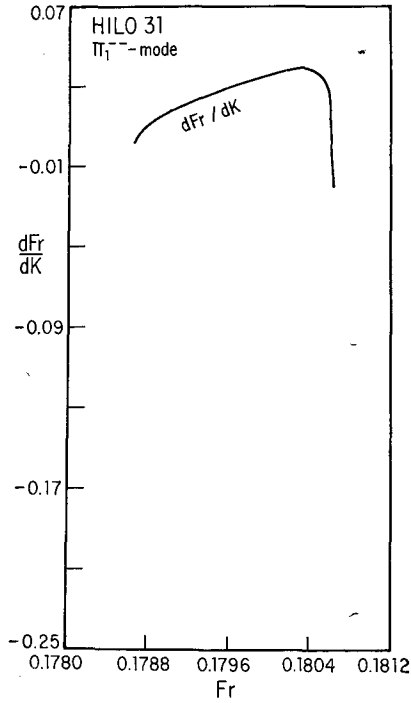


FIG. 19. The derivative dF_r/dK for the Π_1^{+-} -mode. The model is Hilo 31. The group velocity is $g = |dF_r/dK|$.

maximum values are either not affected by attenuation, like Π_1^{--} , Π_2^{--} for Hilo 19 and Π_{17}^{--} for Hilo 31 or they are only slightly reduced, like Π_{11}^{--} for both models (Figures 21, 23). What we mean here by attenuation is only a tentative estimate since exact numerical values for the spatial attenuation can be obtained only if we know exactly what is the distance to the generating area. In order to estimate how attenuation can affect the contribution of the leaking modes we introduced a spatial attenuation factor

$$A = e^{-2} \left(\frac{F_i d}{g} \right) \quad (28)$$

where d is an average distance to the generating area. We took the tentative values: $d = 0.001$ for Hilo 19 and $d = 0.002$ for Hilo 31. The attenuated transfer function is represented in Figures 21, 23. The low frequency Π_i^{--} -modes are almost unchanged, whereas some of the higher frequency Π_i^{--} -modes are strongly affected, but in such a way that the whole picture seems to look more like the measured spectrum.

Obviously, due to imperfections of the theory and great simplifications of the considered models, one cannot expect more than a qualitative picture, but even so, the role of the leaking modes is clearly shown.

ACKNOWLEDGMENTS

I am grateful to Professor Freeman Gilbert for suggesting this problem and for various discussions.

This research has been supported by Air Force Contract AF49(638)-1388. The paper was presented at the 48th Annual Meeting of the American Geophysical Union, held in Washington, D. C., April 17-20, 1967.

REFERENCES

1. Brander, H. and J. G. Dodds (1964). Comparative seismic noise on the ocean bottom and on land, *J. Geophys. Res.* **69**, 4339-4348.
2. Gilbert, F. (1964). Propagation of transient leaking modes in a stratified elastic waveguide, *Rev. Geophys.* **2**, 123-154.
3. Gilbert, F. and G. E. Backus (1966). Propagator matrices in elastic wave and vibration problems, *Geophysics* **31**, 326-332.
4. Gilbert, F. and S. J. Laster (1962). Experimental investigation of *PL* modes in a single layer, *Bull. Seism. Soc. Am.* **52**, 59-66.
5. Hasselmann, K. (1963). A statistical analysis of the generation of microseisms, *Rev. Geophys.* **1**, 177-210.
6. Oliver, J. (1961). On the long period character of shear waves, *Bull. Seism. Soc. Am.* **51**, 1-12.
7. Oliver, J. and M. Major (1960). Leaking modes and the *PL* phase, *Bull. Seism. Soc. Am.* **50**, 165-180.
8. Pekeris, C. L. (1948). Theory of propagation of explosive sound in shallow water, *Geol. Soc. Am., Mem.* **27**, 53 pp.
9. Phinney, R. A. (1961). Leaking modes in the crustal waveguide. Part 1. The Oceanic *PL* wave, *J. Geophys. Res.* **66**, 1445-1469.
10. Pollard, D. D. and J. P. Eaton (1963). Crustal structure of the island of Hawaii. *Abstract Annual Meeting*, Seism. Soc. Am.

11. Rosenbaum, L. H. (1960). The long-time response of a layered elastic medium to explosive sound, *J. Geophys. Res.* **65**, 1577-1613.
12. Shor, G. G. Jr. and D. D. Pollard (1964). Mohole site selection studies north of Maui, *J. Geophys. Res.* **69**, 1627-1637.
13. Su, S. S. and J. Dorman (1965). The use of leaking modes in seismogram interpretation and in studies of crust-mantle structure, *Bull. Seism. Soc. Am.* **55**, 989-1021.

INSTITUTE OF GEOPHYSICS AND PLANETARY PHYSICS
 UNIVERSITY OF CALIFORNIA
 LA JOLLA, CALIFORNIA

Manuscript received September 7, 1967.

APPENDIX A

Reduction of the Differential System

It was shown (Gilbert and Backus, 1966) that if a matrix

$$\mathfrak{F}(y) = (F_{ij}(y)) \tag{A.1}$$

satisfies the differential equation

$$\frac{d\mathfrak{F}(y)}{dy} = \mathfrak{A}(y)\mathfrak{F}(y) \tag{A.2}$$

where

$$\mathfrak{A}(y) = (A_{ij}(y)) \tag{A.3}$$

then the m th order determinants

$$F(\overset{i_1 \dots i_m}{\underset{k_1 \dots k_m}{\epsilon}}) = \sum_{j_1 \dots j_m} F_{i_1 j_1} F_{i_2 j_2} \dots F_{i_m j_m} \epsilon_{\overset{j_1 \dots j_m}{\underset{k_1 \dots k_m}{\epsilon}}} \tag{A.4}$$

are solutions of

$$\frac{dF(\overset{i_1 \dots i_m}{\underset{k_1 \dots k_m}{\epsilon}})}{dy} = \sum_l A_{i_1 l} F(\overset{l \dots i_m}{\underset{k_1 \dots k_m}{\epsilon}}) + \dots + \sum_l A_{i_m l} F(\overset{i_1 \dots l}{\underset{k_1 \dots k_m}{\epsilon}}). \tag{A.5}$$

Here $\overset{i_1 \dots i_m}{\underset{k_1 \dots k_m}{\epsilon}}$ is the mixed complete antisymmetric tensor of order $2m$. Since the coefficients in the right hand side of (A.5) do not depend on the indices K_1, K_m , it follows that this system is satisfied by every column of the matrix $\mathfrak{F}^{(m)}$ the elements of which are all the m th order determinants. In particular, for $n = 4$ and $m = 2$,

$$\frac{d\mathfrak{F}^{(2)}(y)}{dy} = \mathfrak{A}(y)\mathfrak{F}^{(2)}(y) \tag{A.6}$$

where the matrix \mathfrak{A} is (Gilbert and Backus, 1966)

$$\mathfrak{A} = \begin{bmatrix} A_{11} + A_{22} & A_{23} & A_{24} & -A_{13} & -A_{14} & 0 \\ A_{32} & A_{11} + A_{33} & A_{34} & A_{12} & 0 & -A_{14} \\ A_{42} & A_{43} & A_{11} + A_{44} & 0 & A_{12} & A_{13} \\ -A_{31} & A_{21} & 0 & A_{22} + A_{33} & A_{34} & -A_{24} \\ -A_{41} & 0 & A_{21} & A_{43} & A_{22} + A_{44} & A_{23} \\ 0 & -A_{41} & A_{31} & -A_{42} & A_{32} & A_{33} + A_{44} \end{bmatrix} \quad (\text{A.7})$$

There is a very simple algebraic relation between the elements of $\mathfrak{F}^{(2)}(z)$ pertaining to the same column, namely:

$$F_{(\kappa_1 \kappa_2)}^{(12)} F_{(\kappa_1 \kappa_2)}^{(34)} + F_{(\kappa_1 \kappa_2)}^{(23)} F_{(\kappa_1 \kappa_2)}^{(14)} + F_{(\kappa_1 \kappa_2)}^{(31)} F_{(\kappa_1 \kappa_2)}^{(24)} = 0. \quad (\text{A.8})$$

This relation follows from the definition (A.4) of $F_{(\kappa_1 \kappa_2)}^{(i_1 i_2)}$. Using it, the sixth-order system (A.6) can be reduced to one of order four. To show this let us denote the elements of any column of $\mathfrak{F}^{(2)}$ by U_1, \dots, U_6 . Multiplying the first equation (A.6) by $-U_3$, the third by U_1 and adding the results, we get:

$$\begin{aligned} U_1 \frac{dU_3}{dy} - U_3 \frac{dU_1}{dy} &= A_{42} U_1^2 + A_{43} U_1 U_2 + (A_{11} + A_{44}) U_1 U_3 + A_{12} U_1 U_5 \\ &+ A_{13} U_1 U_6 - (A_{11} + A_{22}) U_1 U_3 - A_{23} U_2 U_3 - A_{24} U_3^2 \\ &+ A_{13} U_3 U_4 + A_{14} U_3 U_5. \end{aligned} \quad (\text{A.9})$$

Using now (A.8) and dividing by U_1^2 :

$$\begin{aligned} \frac{d\left(\frac{U_3}{U_1}\right)}{dy} &= A_{42} + A_{43} \frac{U_2}{U_1} + (A_{44} - A_{22}) \frac{U_3}{U_1} + A_{12} \frac{U_5}{U_1} + A_{13} \frac{U_2 U_5}{U_1 U_1} \\ &- A_{23} \frac{U_2 U_3}{U_1 U_1} - A_{24} \left(\frac{U_3}{U_1}\right)^2 + A_{14} \frac{U_3 U_5}{U_1 U_1}. \end{aligned} \quad (\text{A.10})$$

Repeating the same kind of operation on other combinations, we get three more equations:

$$\begin{aligned} \frac{d\left(\frac{U_4}{U_1}\right)}{dy} &= -A_{31} + A_{21} \frac{U_2}{U_1} + (A_{33} - A_{11}) \frac{U_4}{U_1} + A_{34} \frac{U_5}{U_1} - A_{24} \frac{U_2 U_5}{U_1 U_1} \\ &- A_{23} \frac{U_2 U_4}{U_1 U_1} + A_{13} \left(\frac{U_4}{U_1}\right)^2 + A_{14} \frac{U_4 U_5}{U_1 U_1} \end{aligned} \quad (\text{A.11})$$

$$\begin{aligned} \frac{d}{dy} \left(\frac{U_2}{U_1} \right) = & A_{32} + (A_{33} - A_{22}) \frac{U_2}{U_1} + A_{36} \frac{U_3}{U_1} + A_{12} \frac{U_4}{U_1} + A_{14} \frac{U_3}{U_1} \frac{U_4}{U_1} \\ & - A_{23} \left(\frac{U_2}{U_1} \right)^2 - A_{24} \frac{U_2}{U_1} \frac{U_3}{U_1} + A_{13} \frac{U_2}{U_1} \frac{U_4}{U_1} \end{aligned} \quad (\text{A.12})$$

$$\begin{aligned} \frac{d}{dy} \left(\frac{U_5}{U_1} \right) = & -A_{41} + A_{21} \frac{U_3}{U_1} + A_{43} \frac{U_4}{U_1} + (A_{44} - A_{11}) \frac{U_5}{U_1} - A_{23} \frac{U_3}{U_1} \frac{U_4}{U_1} \\ & - A_{24} \frac{U_5}{U_1} \frac{U_3}{U_1} + A_{13} \frac{U_5}{U_1} \frac{U_4}{U_1} + A_{14} \left(\frac{U_5}{U_1} \right)^2. \end{aligned} \quad (\text{A.13})$$

In the particular case when \mathfrak{A} is (B.4),

$$A_{11} = A_{14} = A_{22} = A_{23} = A_{32} = A_{33} = A_{41} = A_{44} = 0 \quad (\text{A.14})$$

and

$$A_{34} = -A_{21}, \quad A_{12} = A_{13}. \quad (\text{A.15})$$

In this case

$$U_5 = -U_2 \quad (\text{A.16})$$

and the system (A.10)-(A.13) is reduced to three equations only. Using the expressions of the elements A_{12} , etc. these equations are:

$$\frac{d}{dy} \left(\frac{U_2}{U_1} \right) = K \frac{U_3}{U_1} + \frac{K\lambda}{\lambda + 2\mu} \frac{U_4}{U_1} - \frac{1}{\mu} \frac{U_2}{U_1} \frac{U_3}{U_1} + \frac{1}{\lambda + 2\mu} \frac{U_2}{U_1} \frac{U_4}{U_1} \quad (\text{A.17})$$

$$\frac{d}{dy} \left(\frac{U_3}{U_1} \right) = X - 2 \frac{K\lambda}{\lambda + 2\mu} \frac{U_2}{U_1} - \frac{1}{\lambda + 2\mu} \left(\frac{U_2}{U_1} \right)^2 - \frac{1}{\mu} \left(\frac{U_3}{U_1} \right)^2 \quad (\text{A.18})$$

$$\frac{d}{dy} \left(\frac{U_4}{U_1} \right) = \rho F^2 - 2K \frac{U_2}{U_1} + \frac{1}{\mu} \left(\frac{U_2}{U_1} \right)^2 + \frac{1}{\lambda + 2\mu} \left(\frac{U_4}{U_1} \right)^2 \quad (\text{A.19})$$

When $K = 0$, X equals $-\rho F^2$ and equations (A.17)-(A.19) become:

$$\frac{d}{dy} \left(\frac{U_2}{U_1} \right) = \left(-\frac{1}{\mu} \frac{U_3}{U_1} + \frac{1}{\lambda + 2\mu} \frac{U_2}{U_1} \right) \frac{U_2}{U_1} \quad (\text{A.20})$$

$$\frac{d}{dy} \left(\frac{U_3}{U_1} \right) = -\rho F^2 - \frac{1}{\lambda + 2\mu} \left(\frac{U_2}{U_1} \right)^2 - \frac{1}{\mu} \left(\frac{U_3}{U_1} \right)^2 \quad (\text{A.21})$$

$$\frac{d}{dy} \left(\frac{U_4}{U_1} \right) = \rho F^2 + \frac{1}{\mu} \left(\frac{U_2}{U_1} \right)^2 + \frac{1}{\lambda + 2\mu} \left(\frac{U_4}{U_1} \right)^2 \tag{A.22}$$

As the initial value of U_2/U_1 is zero, it follows from (A.20) that it vanishes identically, which means that (A.21), (A.22) are reduced to

$$\frac{d}{dy} \left(\frac{U_3}{U_1} \right) = -\rho F^2 - \frac{1}{\mu} \left(\frac{U_3}{U_1} \right)^2 \tag{A.23}$$

$$d \left(\frac{U_4}{U_1} \right) = \rho F^2 + \frac{1}{\lambda + 2\mu} \left(\frac{U_4}{U_1} \right)^2. \tag{A.24}$$

APPENDIX B

The starting values for the integration of the fourth-order differential system (3) are:

$$\begin{aligned} s_y' &= (K^2 - F^2/\alpha_0^2)^{1/2} & s_y'' &= \frac{K}{\mu_0(K^2 - F^2)^{1/2}} \\ s_x' &= K & s_x'' &= 1/\mu_0 \\ \tau_{yy}' &= 2\mu_0 K^2 - F^2\rho_0 & \tau_{yy}' &= 2K \\ \tau_{yx}' &= 2\mu_0 K(K^2 - F^2/\alpha_0^2)^{1/2} & \tau_{yx}' &= -\frac{F^2\rho_0 - 2\mu_0 K^2}{\mu_0(K^2 - F^2)^{1/2}}. \end{aligned} \tag{B.1}$$

The sixth order differential system for the determinants $G(\binom{12}{12})$, etc. is:

$$\frac{d\mathfrak{u}}{dy} = \mathfrak{A}\mathfrak{u} \tag{B.2}$$

where \mathfrak{u} is a one-column matrix having as components the determinants:

$$\mathfrak{u} = \begin{bmatrix} G(\binom{12}{12}) \\ G(\binom{13}{12}) \\ G(\binom{14}{12}) \\ G(\binom{23}{12}) \\ G(\binom{24}{12}) \\ G(\binom{34}{12}) \end{bmatrix}. \tag{B.3}$$

and \mathfrak{A} is the sixth-order matrix:

$$\alpha = \begin{bmatrix} 0 & 0 & \frac{1}{\mu} & -\frac{1}{\lambda + 2\mu} & 0 & 0 \\ 0 & 0 & K & \frac{K\lambda}{\lambda + 2\mu} & 0 & 0 \\ X & -\frac{K\lambda}{\lambda + 2\mu} & 0 & 0 & \frac{K\lambda}{\lambda + 2\mu} & \frac{1}{\lambda + 2\mu} \\ \rho F^2 & -K & 0 & 0 & K & -\frac{1}{\mu} \\ 0 & 0 & -K & \frac{-K\lambda}{\lambda + 2\mu} & 0 & 0 \\ 0 & 0 & -\rho F^2 & -X & 0 & 0 \end{bmatrix}. \quad (\text{B.4})$$

Here

$$X = -\rho F^2 + \frac{4K^2\mu(\lambda + \mu)}{\lambda + 2\mu}. \quad (\text{B.5})$$

The starting values are:

$$\begin{aligned} G_{(12)}^{(12)} &= \frac{\nu_P \nu_S - K^2}{\mu_0 \nu_S} \\ G_{(12)}^{(13)} &= K \frac{2\mu_0 \nu_P \nu_S - (2\mu_0 K^2 - F^2 \rho_0)}{\mu_0 \nu_S} \\ G_{(12)}^{(14)} &= -\frac{F^2 \rho_0 \nu_P}{\mu_0 \nu_S} \\ G_{(12)}^{(23)} &= -\frac{F^2 \rho_0}{\mu_0} \\ G_{(12)}^{(24)} &= -G_{(12)}^{(13)} \\ G_{(12)}^{(34)} &= \frac{(2\mu_0 K^2 - F^2 \rho_0)^2 - 4K^2 \mu_0^2 \nu_P \nu_S}{\mu_0 \nu_S} \end{aligned} \quad (\text{B.6})$$

where

$$\nu_P = (K^2 - F^2/\alpha_0^2)^{1/2}, \quad \nu_S = (K^2 - F^2)^{1/2}. \quad (\text{B.7})$$

The derivatives with respect to the frequency F are solutions of

$$\frac{d(d\mathbf{u}/dF)}{dy} = \frac{d\alpha}{dF} \mathbf{u} + \alpha \frac{d\mathbf{u}}{dF} \quad (\text{B.8})$$

u satisfying (B.2). The starting values for the derivatives are:

$$\begin{aligned} \frac{dG(\overset{12}{12})}{dF} &= -\frac{F}{\mu_0} \left(\frac{1}{\alpha_0^2 \nu_P} + \frac{K^2}{\beta_0^2 \nu_S^3} \right)^\dagger \\ \frac{dG(\overset{13}{12})}{dF} &= KF \left(-\frac{2}{\alpha_0^2 \nu_P} + \frac{2\rho_0}{\mu_0^2 \nu_S} - \frac{2\mu_0 K^2 - F^2 \rho_0}{\mu_0 \beta_0^2 \nu_S^3} \right) \\ \frac{dG(\overset{14}{12})}{dF} &= -\frac{\rho_0 F}{\mu_0 \nu_P \nu_S} \left[2\nu_P^2 \nu_S^2 + K^2 \left(\frac{F^2}{\beta_0^2} - \frac{F^2}{\alpha_0^2} \right) \right] \\ \frac{dG(\overset{23}{12})}{dF} &= \frac{2\rho_0 F}{\mu_0} \\ \frac{dG(\overset{24}{12})}{dF} &= -\frac{dG(\overset{13}{12})}{dF} \\ \frac{dG(\overset{34}{12})}{dF} &= F \left[\frac{(2\mu_0 K^2 - F^2 \rho_0) \left(3\rho_0 \frac{F^2}{\beta_0^2} - 4\rho_0 K^2 + \frac{2\mu_0 K^2}{\beta_0^2} \right)}{\mu_0 \nu_S^3} + \frac{4K^2 \mu_0}{\alpha_0^2 \nu_P} \right]. \quad (\text{B.9}) \end{aligned}$$

The derivatives with respect to the wave-number K are solutions of a differential system similar to (B.8). Their initial values are:

$$\begin{aligned} \frac{dG(\overset{12}{12})}{dK} &= \frac{K}{\mu_0} \left(\frac{1}{\nu_P} - \frac{1}{\nu_S} + \frac{F^2}{\beta_0^2 \nu_S^3} \right) \\ \frac{dG(\overset{13}{12})}{dK} &= 2 \left(\nu_P + \frac{K^2}{\nu_P^2} \right) - 4 \frac{K^2}{\nu_S} + \frac{(2\mu_0 K^2 - F^2) F^2}{\beta_0^2 \mu_0 \nu_S^3} \\ \frac{dG(\overset{14}{12})}{dK} &= \frac{KF^4 \rho_0 (\alpha_0^2 - \beta_0^2)}{\mu_0 \alpha_0^2 \beta_0^2 \nu_P \nu_S^3} \\ \frac{dG(\overset{23}{12})}{dK} &= 0 \\ \frac{dG(\overset{24}{12})}{dK} &= -\frac{dG(\overset{13}{12})}{dK} \\ \frac{dG(\overset{34}{12})}{dK} &= K \left[(2\mu_0 K^2 - F^2 \rho_0) \left(\frac{8}{\nu_S} - \frac{2\mu_0 K^2 - F^2 \rho_0}{\mu_0 \nu_S^3} \right) - 4\mu_0 \left(2\nu_P + \frac{K^2}{\nu_P} \right) \right]. \quad (\text{B.10}) \end{aligned}$$

† We wrote here β_0 for convenience.